UCLA
UCLA Previously Published Works

Title

Catalytic Asymmetric Hydrogen Atom Transfer: Enantioselective Hydroamination of Alkenes.

Permalink

https://escholarship.org/uc/item/7vv4w4xj

Journal

Journal of the American Chemical Society, 145(29)

Authors

Hejna, Benjamin
Ganley, Jacob
Shao, Huiling
et al.

Publication Date

2023-07-26

DOI

10.1021/jacs.3c04591

Peer reviewed

eScholarship.org Powered by the California Digital Library
University of California

Author Manuscript

Author Manuscript

Author Manuscript

Author Manuscript

HHS Public Access

Author manuscript

J Am Chem Soc. Author manuscript; available in PMC 2024 July 26.

Published in final edited form as:

J Am Chem Soc. 2023 July 26; 145(29): 16118–16129. doi:10.1021/jacs.3c04591.

Catalytic Asymmetric Hydrogen Atom Transfer: Enantioselective Hydroamination of Alkenes

Benjamin G. Hejna[†], **Jacob M. Ganley**[†], **Huiling Shao**[‡], **Haowen Tian**[‡], **Jonathan D. Ellefsen**[#], **Nicholas J. Fastuca**[†], **K. N. Houk**[‡], **Scott J. Miller**[#], **Robert R. Knowles**[†]

[†]Department of Chemistry, Princeton University, Princeton, New Jersey 08544, United States

[‡]Department of Chemistry and Biochemistry, University of California, Los Angeles, California 90095, United States

[#]Department of Chemistry, Yale University, New Haven, Connecticut 06520, United States

Abstract

We report a highly enantioselective radical-based hydroamination of enol esters with sulfonamides jointly catalyzed by an Ir photocatalyst, Brønsted base, and tetrapeptide thiol. This method is demonstrated for the formation of 23 protected β-amino-alcohol products, achieving selectivities up to 97:3 er. The stereochemistry of the product is set through selective hydrogen atom transfer from the chiral thiol catalyst to a prochiral *C*-centered radical. Structure-selectivity relationships derived from structural variation of both the peptide catalyst and olefin substrate provide key insights into the development of an optimal catalyst. Experimental and computational mechanistic studies indicate that hydrogen-bonding, π-π stacking, and London dispersion interactions are contributing factors for substrate recognition and enantioinduction. These findings further the development of radical-based asymmetric catalysis and contribute to the understanding of the noncovalent interactions relevant to such transformations.

Graphical Abstract

Corresponding Authors: **K. N. Houk** – Department of Chemistry and Biochemistry, University of California, Los Angeles, California 90095, United States. houk@chem.ucla.edu, **Scott J. Miller** – Department of Chemistry, Yale University, New Haven, Connecticut 06511, United States. scott.miller@yale.edu, **Robert R. Knowles** – Department of Chemistry, Princeton University, Princeton, New Jersey 08544, United States. rknowles@princeton.edu.

The authors declare no competing financial interests.

ASSOCIATED CONTENT

Supporting Information

The Supporting Information is available free of charge on the ACS Publications website.

Experimental details, crystallographic and computational information, NMR spectra, and HPLC traces (PDF)

Crystal structure of **P4** (CIF)

Crystal structure of **P14** (CIF)

Crystal structure of **5d** (CIF)

Author Manuscript Author Manuscript Author Manuscript Author Manuscript

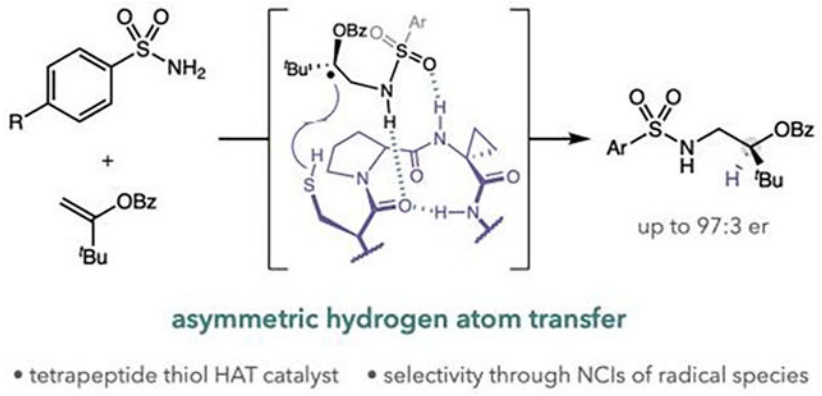

INTRODUCTION

Over the last decade, the development of synthetic methods that utilize free radical intermediates has progressed at a remarkable rate. Key to these advances has been the widespread adoption of photoredox catalysis, which facilitates the generation of radical intermediates under mild conditions.[1] This tunable approach to radical generation has further enabled the development of catalytic protocols which proceed with outstanding chemoselectivity, regioselectivity, and enantioselectivity. As part of this development, a wide variety of chiral catalysts have been successfully applied to asymmetric functionalization of *C*–centered radicals, effecting the formation of C–C, C–N, C–O, and C–M bonds, among others.[2] Despite this progress, catalytic methods for asymmetric hydrogen atom transfer (HAT) to form the analogous C–H bond are notably scarce.

While HAT to a *C*-centered radical is a common elementary step in many radical transformations, several inherent features of HAT have hindered the development of stereoselective variants (Figure 1a).[3] Favorable HAT reactions typically exhibit early transition states wherein the incipient C–H bond is elongated.[4] Along with a linear arrangement of participating atoms, this positions the stereochemical information of a chiral H-atom donor distal to the site of reactivity. Additionally, the potential for racemic background HAT can pose a challenge and must be accounted for. Most successful efforts in this field utilize chiral Lewis acids or complexing reagents, which form ordered complexes with radical intermediates and template their stereoselective reactions with achiral H-atom donors (Figure 1b).[5,6]

Many fewer examples have been demonstrated using H-atom donors which are themselves chiral.[7] Early studies utilized chiral stannane reagents as stoichiometric H-atom donors, and while some of these reagents mediate reduction with high enantioselectivity, catalytic variants are rare and have not achieved such high levels of selectivity (Figure 1b).[8] In 1998, Roberts and coworkers utilized chiral carbohydrate-derived thiol catalysts to achieve enantioselective HAT in the context of asymmetric alkene hydrosilylation (Figure 1b).[9] This report stands as the first example of a highly enantioselective catalytic HAT process. However, only a single hydrosilylation product was generated in >95:5 er. Addressing this limitation, the Ye group recently reinvestigated this thiosugar-catalyzed system in a

Author Manuscript Author Manuscript Author Manuscript Author Manuscript

photochemical deuterosilylation protocol, demonstrating high enantioselectivity across a significantly expanded scope.[10]

In biological systems, enzymes are known to effectively deliver a H-atom to radicals with remarkably high degrees of stereoselectivity, as seen in ribonucleotide reductases and radical *S*-adenosyl methionine epimerases.[11] These protein catalysts are understood to precisely bind and orient open-shell intermediates within their active sites such that a suitably positioned residue or cofactor transfers a H-atom to a single face of the radical with high selectivity.[12] To this end, the Hyster and Zhao groups have effectively applied evolved ene-reductases to a suite of biocatalytic transformations that leverage HAT as the enantiodetermining step (Figure 1c).[13]

Taking these works into consideration, we became interested in developing small molecule peptide catalysts that could be applied in catalytic asymmetric HAT protocols. These peptide organocatalysts are highly modular and endeavor to recapitulate key mechanistic features of enzymes, employing cooperative noncovalent interactions (NCIs) to achieve high levels of stereoselectivity.[14] As such, our laboratories collectively demonstrated the deracemization of cyclic ureas using an Ir(III) photocatalyst, a chiral phosphate base, and a cysteine-based peptide asymmetric HAT catalyst.[15] This method achieves enantioselectivities up to 96:4 er due to a multiplicative effect of key enantioselective proton transfer and HAT elementary steps. Both of these steps exhibit moderate enantioselectivities in isolation, with up to 85:15 er for the HAT step. Having established the viability of this class of catalysts for HAT, we sought to develop a peptide thiol catalyst which individually effects highly enantioselective HAT. With regard to this, we highlight a recent study from Ye and coworkers, which demonstrated the use of similar peptide thiol catalysts for enantioselective deuterium atom transfer.[16] In this report, we describe the development of a system for enantioselective alkene hydroamination, in which asymmetric HAT from a cysteine-bearing tetrapeptide enables the formation of amino-alcohol derivatives with high degrees of optical enrichment (Figure 1d). We then provide a series of experimental and computational mechanistic studies which culminate in a detailed stereochemical model for the key HAT step.

RESULTS AND DISCUSSION

To enable this peptide-mediated asymmetric HAT step, we considered catalytic systems that generate the necessary prochiral *C*-centered radical. Accordingly, we chose to adapt a light-driven olefin hydroamination protocol previously reported by Knowles and coworkers.[17] In this transformation, an excited state Ir photocatalyst and Brønsted base mediate the homolysis of a sulfonamide N–H bond *via* concerted proton-coupled electron transfer (PCET). The resultant *N*-centered radical then undergoes anti-Markovnikov addition to a 1,1-disubstituted alkene, furnishing a new C–N bond and a prochiral *C*-centered radical. In the original report, an achiral thiol co-catalyst was employed to catalyze a racemic HAT step and afford the desired hydroamination product. We reasoned that this reaction could be rendered asymmetric through substitution of the thiophenol catalyst for a peptide-based thiol, thereby providing a platform for the development and study of this class of chiral HAT catalysts (Figure 1d).

Author Manuscript Author Manuscript Author Manuscript Author Manuscript

As such, we began our investigation by evaluating the performance of a suite of cysteine-containing peptide thiols as HAT co-catalysts in this hydroamination reaction. Our initial efforts focused on the hydroamination of isopropenyl acetate (**2**) with 4-methoxybenzenesulfonamide (**1a**) mediated by a ternary catalyst system comprised of $[Ir(dF\text{-}CF_3\text{-}ppy)_2(5,5'\text{-}d(CF_3)bpy)]PF_6$ (**Ir**) as a photocatalyst, $[PBu_4]OC(CF_3)_3$ as a Brønsted base catalyst, and a peptide thiol HAT catalyst under blue light irradiation in toluene at 30 °C. Under these conditions, we observed that tetrapeptide thiol Boc-Cys-^{D}Pro-Acpc-Phg-NMe_2 (**P1**) provided hydroamination product **3** in 30% yield and an encouraging 76:24 er (Figure 2). With this preliminary result in hand, we evaluated a library of derivatives of **P1**, seeking to systematically modify each position of the peptide to gain insight into the role of each residue.

Peptide Structure-Selectivity Studies.

Tetrapeptides with β-turn-biased primary sequences have been established as effective catalysts for asymmetric catalysis.[14] This motif is characterized by a hydrogen-bonding interaction between the carbonyl group of the *N*-terminal (*i*) residue (bearing the catalytic functionality) and the N–H bond of the *C*-terminal (*i*+3) residue. The combination of a proline-type residue at the *i*+1 position and an α,α-disubstituted residue at the *i*+2 position nucleates this interaction, thereby bringing the functionality of the catalyst into proximity with the substrate and fostering NCIs.[19,20]

A variety of secondary structures that contain a generalized β-turn motif are known, and the exact secondary structure has a significant impact on the peptide's enantiodiscrimination of prochiral intermediates.[21] Notably, the identity of the *i*+2 residue is well-understood to exert a strong influence on the secondary structure of tetrapeptides.[22] Therefore, we began our structure-selectivity relationship studies by evaluating peptides **P1**–**P4**, which exhibit structurally diverse *i*+2 residues (Figure 2). In this series, peptides with small-ring residues (Acpc: **P1** and Acbc: **P4**) underwent HAT with higher enantioselectivity than those with an acyclic (Aib: **P2**) or larger-ring (Cle: **P3**) residue. Previous studies of similar tetrapeptides have shown that residues containing smaller rings such as Acpc or Acbc display larger τ angles; consequently, peptides bearing these residues at the *i*+2 position exhibit larger binding sites, distancing the *i*+3 residue from the catalytic *i* residue.[21c] This research also determined that peptides which employ *i*+2 residues with larger τ angles demonstrate increased conformational flexibility. For a set of related sequences with ^{D}Pro at the *i*+1 position, congeners with Acpc and Acbc at the *i*+2 position were found to access both type I' and type II' β-turns (differentiated by an amide plane flip of the peptide bond between the *i*+1 and *i*+2 residues, i.e. $\varphi_{i+2} \sim \pm 90°$) in the solution phase.[21c] Meanwhile, peptides bearing Aib or Cle are less flexible and were demonstrated to exhibit fewer conformations in the solution state. In this hydroamination system, it is plausible that the Acpc residue of **P1** is optimal due to the combination of a more accessible binding site and additional catalyst flexibility.

To further investigate the effect of the *i*+2 residue on enantioselectivity, we evaluated peptide **P5** which contains dehydrovaline (Dhv). This residue displays a large τ angle (~120°), but **P5** was unselective (49:51 er). The incorporation of an additional sp^2-hybridized atom

Author Manuscript Author Manuscript Author Manuscript Author Manuscript

into the peptide backbone introduces rigidity and allylic strain, thereby restricting the conformational space available to the peptide.[23] It is thus likely that **P5** cannot adopt a selective conformation analogous to that of **P1**. Indeed, for catalysts such as peptides that rely on NCIs for enantiodifferentiation, it is increasingly appreciated that conformational flexibility allows for reorganization of these NCIs into maximally stable geometries along a complex reaction coordinate.[24] The results obtained with peptides **P1**–**P5** are consistent with this theory.

At this point, we sought to gain insight into the preferred conformation of **P1**. While attempts to crystallize **P1** were unsuccessful, we were able to obtain a crystal of similarly selective Acbc-based **P4** which was suitable for analysis by X-ray diffraction (Figure 2). The crystal structure of **P4** exhibits a type II' β-hairpin secondary structure, which places the i+1/i+2 amide N–H bond on the same face of the peptide as the thiol group where HAT is expected to occur. Solution phase ^{1}H-^{1}H NOESY studies show a strong NOE between this N–H bond and the α-proton of the ^{D}Pro residue, consistent with this secondary structure (see SI Section S8). Taking these data into account with prior studies of peptide catalysts bearing similar primary sequences, we expect that this type II' β-hairpin conformation contributes significantly to the ensemble of possible HAT transition states.[21c]

Having established Acpc as the optimal i+2 residue, we next studied the i+3 residue of the peptide thiol catalyst. To probe the role of this residue, we evaluated peptides **P6**–**P12** which bear Acpc at the i+2 position and structurally diverse i+3 residues. Examining peptides **P6**–**P9** alongside **P1**, it became clear that phenylglycine (Phg - **P1**) is the optimal i+3 residue in this system (Figure 2). Replacement of Phg with structurally similar residues, such as the saturated analog Chg (**P6**), homolog Phe (**P7**), or epimer ^{D}Phg (**P8**) resulted in significantly diminished enantioselectivities. We hypothesized that the π-system of the Phg residue may be involved in a NCI in the HAT transition state, and so we tested peptide **P10** bearing an extended π-surface area, as well as **P11** and **P12** bearing electron-rich and electron-poor Phg derivatives, respectively (Figure 2). Interestingly, **P10**–**P12** all performed almost identically to **P1**, suggesting a more complex role for the Phg residue.

We also evaluated analogous peptides with variations at the i residue, the i+1 residue, and the C- and N-terminal protecting groups. However, all meaningful structural changes caused either no significant change in or diminished enantioselectivity compared to **P1**.

Effect of Olefin Substitution.

Having identified a lead catalyst (**P1**), we opted to study the structure-selectivity relationship of the substrate substituents. We first tested the efficacy of isopropenyl benzoate (**4a**) and found it to perform comparably to isopropenyl acetate, providing product **5a** in 77:23 er (Figure 3). Continuing with vinyl benzoate-derived substrates, we observed improvements in enantioselectivity with increasing substitution on the carbon atom vicinal to the nascent stereocenter (**5a**–**5c**). However, this trend does not hold for the *tert*-butyl substituted enol benzoate **4d**, which provided **5d** with diminished 79:21 er at 30 °C. Decreasing the reaction temperature led to increased enantioselectivity for all substrates, although the degree of this effect varied based on the substituent and was particularly pronounced for **5d**. During

Author Manuscript Author Manuscript Author Manuscript Author Manuscript

these variable temperature studies, we observed that peptide catalyst **P1** was only sparingly soluble in toluene at –10 °C at the reaction concentration (10 mM). This led to poor reaction reproducibility and precluded reliable mechanistic studies. As such, we sought to design a catalyst that was completely soluble at cryogenic temperatures.

Peptide Optimization.

In preliminary evaluation of catalyst structural motifs (**P2**–**P12**), most modifications to **P1** proved to be detrimental. However, *para*-substitution of the *i*+3 Phg residue arene had almost no influence on reaction enantioselectivity (**P11**, **P12**). We therefore chose to modify this site to achieve a more soluble catalyst. *O*-Alkylation of 4-hydroxyphenylglycine provided straightforward access to peptides with nonpolar groups that enhance solubility in toluene, such as **P13** bearing a 4-heptyloxy group (Figure 4).

Indeed, peptide **P13** was completely soluble under cryogenic reaction conditions. While we anticipated that **P13** would improve the reaction yield and reproducibility, we were surprised to also observe enhanced enantioselectivity relative to **P1**. Seeking to build upon this result, we synthesized **P14**, effectively expanding the 4-heptyloxy group of Yields and enantioselectivities are for isolated material and are the average of two experiments. Reactions were conducted on 0.3 mmol scale using 5 equiv. olefin. Ar = 4-(^{n}BuO)Ph. The X-ray crystal structure of **5d** was rendered using CYLview.[18] [a]using 2 mol% **P14** [b]using 2 equiv. olefin [c]using 5 mol% **P13** [d]using ***ent*-P14 P13** to a dicyclohexylmethyl ether group. When employing **P14** in the hydroamination protocol at –10 °C, we obtained higher selectivity still, observing formation of **5d** with excellent er of 97:3. Through a combination of peptide structure-selectivity studies, substrate modifications, lowering temperature, and peptide alkylation, we developed a peptide thiol which catalyzes an asymmetric HAT step in excellent enantioselectivity.

With **P14** in hand, we next optimized the yield of the hydroamination protocol. Upon translation to preparative scale (0.3 mmol sulfonamide), we observed comparable yield and enantioselectivity to analytical scale (0.05 mmol sulfonamide) with a reaction time of 48 hours under otherwise identical conditions. We then found that decreasing the **Ir** loading to 1 mol% and increasing the olefin loading to 5 equivalents resulted in a significant improvement in reaction yield, delivering product **5d** in 66% yield and 96.5:3.5 er (see SI Section S5 for complete optimization details).

Substrate Scope.

Having identified a highly enantioselective peptide catalyst and optimized reaction conditions for asymmetric hydroamination, we evaluated the substrate scope of this method (Table 1). A variety of (hetero)aryl sulfonamides performed well in this protocol. Benzenesulfonamides featuring ether (**5d**, **5e**, **5m**), silyl ether (**5f**), alkyl (**5g**), trimethylsilyl (**5h**), and sulfide (**5i**–**j**) functionalities at the *para*-position underwent hydroamination effectively, providing access to a variety of protected *β*-amino alcohols in moderate to good yields and with high enantioselectivities. Gratifyingly, methoxy-substituted product **5d** was found to be crystalline, and absolute configuration was determined to be (*S*) by single crystal X-ray diffraction. Heterocyclic sulfonamides, such as thiophene-2-sulfonamide (**5k**)

Author Manuscript Author Manuscript Author Manuscript Author Manuscript

and a pyridine-based sulfonamide (**5l**) underwent hydroamination with good levels of enantioselectivity. **5l** is especially notable, given the potential for the pyridine moiety to interrupt the hydrogen-bonding network which is posited to be responsible for facial discrimination.[25] Electron-poor, *meta*-, or *ortho*-substituted aryl sulfonamides exhibited significantly diminished reactivity and/or selectivity (see SI Table S4).

With 4-*n*-butoxybenzene sulfonamide (**1b**) as a representative sulfonamide, we found that several enol esters were effective as olefin substrates (Table 1). Both electron-rich and electron-poor benzoates underwent hydroamination effectively, although electron-rich substrates (**5n**–**o**) provided improved reactivity and selectivity relative to electron-poor substrates (**5p**–**r**). Substitution at the *ortho* positions of the benzoate (**5s**) was well-tolerated, as was replacement of the phenyl group with thiophene (**5t**). While benzoates were found to be the optimal protecting groups, an enol pivalate also performed well when the olefin was substituted with a cyclohexyl group (**5u**). Enol benzoates bearing *tert*-butyl (**5e**), cyclohexyl (**5v**), bicyclo[2.2.2]octyl (**5w**), and adamantyl (**5x**) groups underwent hydroamination in good yields and high enantioselectivities. We note that the enol ester moiety was critical to achieve good levels of enantioselectivity; modifying the location of the ester or removing it altogether resulted in poor selectivity.

While the highest yields were observed when using 5 equivalents of olefin, practical yields were still obtained with only 2 equivalents (especially for more nucleophilic olefins, as for product **5n**). Similarly, while 5 mol% peptide thiol was employed for the standard conditions, the hydroamination typically proceeded with comparable yield and er with peptide catalyst loadings as low as 2 mol%, as demonstrated for substrate **5e**. Additionally, we investigated the influence of a chiral center vicinal to the site of HAT on the stereoselectivity of the transformation. Employing an enantiopure olefin under our optimized conditions, we obtained the (*S,S*) diastereomer **5y** in 10.3:1 dr. When the enantiomer of **P14** (***ent*-P14**) was used with the same olefin, the (*R,S*) diastereomer **5z** was observed as the major stereoisomer (5.3:1 dr). Notably, an identical reaction employing achiral 1-octanethiol resulted in formation of products **5y** and **5z** in 2.1:1 dr, favoring **5y**. These results highlight the potential of this class of peptide catalysts to exert catalyst-based stereocontrol and override inherent stereochemical preferences of chiral substrates.

Experimental Mechanistic Studies.

Next, we turned our focus towards studying the key NCIs between the peptide catalyst and substrate radical that govern enantioselectivity. In examining the scope of this transformation, we noted the need for an ester moiety to achieve high enantioselectivity. More specifically, electron-rich benzoates generally led to better enantiodiscrimination (Table 1, **5n**–**r**). As peptide catalysts are proposed to interact with their substrates through hydrogen-bonding and other electrostatically-driven NCIs, we conducted a Hammett study to interrogate the participation of the benzoate in such an interaction. Evaluating eight *para*-substituted enol benzoates under standard conditions, we observed an inverse relationship ($\rho = -0.47$) between σ_p and log(er) (Figure 5). This observation indicates that the benzoate moiety indeed participates in an electrostatic interaction during HAT and plays a role in enantioinduction. The observed inverse correlation is consistent with a hydrogen-bonding

Author Manuscript Author Manuscript Author Manuscript Author Manuscript

event through the carbonyl of the benzoate or a π-interaction *via* the benzoate arene, though other modes of electrostatic stabilization are possible.[26]

Given that cyclohexyl groups cannot participate in the electrostatic interactions typically associated with peptide catalysts, we were interested in experimentally probing how the alkyl groups of **P14** improved selectivity relative to **P1**. Our initial hypothesis was that the bulky cyclohexyl groups prevent the formation of aggregated peptide species that undergo HAT to the *C*-centered radical intermediate with diminished selectivity. However, the absence of any nonlinear effects at 30 °C or –10 °C indicate that catalyst aggregation is unlikely (see SI Figures S4 and S5). We also reasoned that aliphatic groups on the periphery of the peptide could induce a change in the catalyst secondary structure, altering the binding mode between the radical intermediate and catalyst. However, NMR spectroscopic studies and X-ray crystallography indicate that the ground state conformations of **P1** and **P14** are very similar (see SI Section S8 and S9). Due to the transient nature of the relevant intermediates, we were unable to experimentally study the exact conformational effect of the dicyclohexylmethyl ether moiety of **P14** upon association with the substrate radical.

Without explicit evidence to define a conformational consequence of the appended cyclohexyl groups, we instead questioned whether the improved selectivity is a result of some stabilizing or destabilizing interaction between the prochiral radical intermediate and the cyclohexyl groups of **P14**. The increased enantioselectivity of **P14** relative to **P1** is a manifestation of the increased $\Delta\Delta G^{\ddagger}$ between the diastereomeric transition states leading to the (*S*)-**5e** or (*R*)-**5e** products. This can be achieved by either raising the barrier to formation of the minor enantiomer relative to that of the major enantiomer or lowering the barrier to formation of the major enantiomer relative to that of the minor.[27] Typically, these two scenarios can be distinguished by comparing the relative rates of the two catalysts, wherein an accelerated reaction rate with the more selective catalyst indicates a stabilizing interaction.[28] However, we observed a zeroth-order kinetic dependence on the concentration of **P14** in the hydroamination reaction (see SI Figure S6). This observation is in line with prior kinetic studies of similar photocatalytic hydroamination reactions, which indicated that thiol-mediated HAT occurs after rate-determining C–N bond formation.[29] As the peptide thiol is not involved in the rate-determining step, the overall reaction rates do not reflect the differential barriers for the competing HAT transition states.

To ascertain the role of the cyclohexyl groups, we instead designed a competition experiment between catalyst **P14** and related catalyst **P15**, which bears an –O^{i}Pr group at the 4-position of the Phg residue arene (Figure 6). **P15** furnishes **5e** with similar selectivity to **P1**, but it exhibits full solubility under the reaction conditions and bears an arene that is electronically comparable to that of **P14** (Figure 6). Under standard reaction conditions, a 1:1 mixture of **P14** and **P15** was utilized in the hydroamination procedure. If the overall rates of HAT for catalysts **P14** and **P15** were identical, then a statistical 95.0:5.0 er would be expected for **5e**, resultant of an average of the selectivities exhibited by each catalyst. However, we found that the composite selectivity for the catalyst mixture was greater than the statistical outcome and was biased towards **P14**. HAT from the more selective catalyst **P14** was thus determined to be *faster* by a factor of approximately 2.2. The presence of the cyclohexyl groups therefore lowers the barrier for the major HAT transition

Author Manuscript Author Manuscript Author Manuscript Author Manuscript

state, which reasonably occurs *via* stabilizing NCIs (see SI Table S8 for calculations of relative rates). We also carried out the same experiment at both high dilution and at room temperature to evaluate potential aggregation and temperature contributions, and in all cases, we reproducibly observed rate acceleration by a factor of 2.1–2.7 (see SI Tables S9–S11). These findings indicate that incorporating the dicyclohexylmethyl ether moiety into the peptide structure leads to a stabilization of the pro-(*S*) HAT transition state relative to the pro-(*R*) transition state. Consequently, we hypothesize that this group contributes to stabilizing NCIs in the dominant transition structure.

Computational Studies.

To gain a better understanding of the NCIs responsible for enantioselectivity in the HAT step, we conducted DFT calculations. All calculations were performed using Gaussian 16.[30] Geometry optimizations were performed using the dispersion-corrected ωB97xd functional[31] with def2SVP basis set,[32] and single point energies were calculated with the ωB97xd functional and the def2TZVP basis set.[32] We benchmarked multiple DFT functionals and basis sets for single-point calculations, and every computational method evaluated resulted in the experimentally observed (*S*)-selectivity. Solvation effects were included by performing single point energy calculations with the CPCM solvation model[33] in toluene ($\varepsilon = 2.37$).[34] Detailed conformational searches on key intermediates were performed using CREST (see SI Tables S13–S16).[35] Only the lowest energy conformations are included in this analysis. To better approximate enthalpies and Gibbs free energies, we applied the quasiharmonic approximation from Grimme to compute the thermal corrections with a cut-off frequency of 50 cm^{-1}.[36] These quasiharmonic approximations were calculated using GoodVibes.[37]

Initially focusing on peptide **P1**, we carried out extensive conformational sampling from which we identified the lowest energy conformer with a *β*-turn/*β*-hairpin secondary structure. We carried out identical sampling for the prochiral *C*-centered radical species **6**. This species favored a conformation stabilized by a π-π stacking interaction between the arene rings of the benzoate and benzenesulfonamide groups (see SI Figure S7 for computational analysis of formation of this radical species).

We next modeled the reaction coordinate profile with **6** and **P1** to study the origin of enantioselectivity in the HAT step. Complexation of the radical and peptide species resulted in the intermediates ***si*-7** and ***re*-7** (Figure 7a). In both intermediates, we identified two hydrogen bonds between the sulfonamide moiety and the peptide: a primary hydrogen bond between the sulfonamide oxygen and $N–H_{Acpc}$ (green) and a secondary hydrogen bond between the sulfonamide N–H and the carbonyl of the Cys residue (pink). ***Si*-7** also contains a third, weak hydrogen bond between the benzoate ester and $S–H_{Cys}$ (blue). Importantly, the key intramolecular π-π stacking interaction observed in **6** is preserved in ***si*-7**, resulting in a small substrate distortion energy (5.8 kcal/mol). However, this interaction is absent in ***re*-7**, leading to significantly higher substrate distortion energy (10.6 kcal/mol). This distortion-interaction analysis thereby suggests that this π-π stacking interaction plays a key role in the preferential formation of ***si*-7** and leads to a more negative binding energy (–22.4 kcal/mol for ***si*-7**, –18.7 kcal/mol for ***re*-7**). In the subsequent selectivity-determining hydrogen atom

Author Manuscript Author Manuscript Author Manuscript Author Manuscript

transfer transition state, this π-π stacking interaction remains intact in **(*S*)-TS1** but absent in **(*R*)-TS1**. We thus hypothesize that this interaction is primarily responsible for the 2.2 kcal/mol stabilization of **(*S*)-TS1** relative to **(*R*)-TS1**. This interaction is also consistent with our Hammett study (Figure 5), providing physical basis to this experimentally observed trend.

Finally, we probed the origin of improved selectivity with **P14** as compared to **P1**. The key dicyclohexylmethyl ether group of **P14** was incorporated into the **(*S*)-TS1** and**(*R*)-TS1** structures, resulting in **(*S*)-TS2** and **(*R*)-TS2**, with **(*S*)-TS2** again favored over **(*R*)-TS2** (Figure 8). Although the computational analysis overestimates the experimentally observed enantioselectivity ($\Delta\Delta G^{\ddagger}_{exp}$ = 1.7 kcal/mol, $\Delta\Delta G^{\ddagger}_{comp}$ = 4.2 kcal/mol), all computational methods tested predict enantioselectivity favoring the experimentally observed **(*S*)-8** product (see SI Table S12).[38] Distortion-interaction analysis revealed that the absence of the key intramolecular π-π stacking interaction in **(*R*)-TS1** and **(*R*)-TS2** leads to larger substrate distortion energy, which favors the (*S*)-selective pathway. In addition to the substrate distortion energy, the interaction energies between the peptide and the substrate contributed more significantly to the observed enantioselectivity with **P14** than with **P1** ($\Delta E_{interaction}$ = 2.4 kcal/mol vs. 0.6 kcal/mol). Taken together with experimental competition studies (Figure 6), these computational results suggest that the dicylohexylmethyl ether group of **P14** leads to a stronger stabilizing interaction between the radical intermediate **6** and **P14** in the major transition state **(*S*)-TS2**.

Based on the transition state geometries, we propose that the stabilizing interaction arises from an NCI between the cyclohexyl groups of **P14** and the arene rings of the substrate. In both **TS2** structures, one cyclohexyl group is closely positioned to the substrate arene(s), which is consistent with London dispersion interaction.[39] The significance of dispersion interactions in asymmetric catalysis is increasingly recognized, particularly in peptide-mediated asymmetric transformations.[40] In this system, we propose that this dispersion interaction is a component of the more favorable interaction energy observed for the **TS2** structures relative to the corresponding **TS1** structures. Furthermore, we note that **(*S*)-TS2** shows three close intermolecular H–H contacts (≤2.3 Å) between the peptide cyclohexyl group and substrate arene, whereas **(*R*)-TS2** displays just one of these close H–H contacts. We also conducted NCIPLOT analysis, which demonstrates the presence of both this dispersive interaction and the aforementioned π-π stacking interaction in **(*S*)-TS2** (see SI Figure S9).[42] These geometries, together with the understanding that larger alkyl groups both are better dispersive donors[41] and provide increased enantioselectivity (Figure 4, **P14** > **P13** > **P1**), lead us to hypothesize that such dispersive interactions contribute to the experimentally and computationally observed increased stabilization of **(*S*)-TS2** relative to **(*R*)-TS2**.[43]

CONCLUSIONS

In summary, we have developed a chiral tetrapeptide thiol catalyst that effects highly selective asymmetric HAT to a prochiral carbon-centered radical, enabling the enantioselective hydroamination of enol esters with sulfonamides. A series of peptide site modifications led to identification of the crucial residues that make for an effective catalyst

Author Manuscript Author Manuscript Author Manuscript Author Manuscript

scaffold, which was further improved by the addition of a dicyclohexylmethyl ether. This protocol was applied to a variety of sulfonamide and olefin partners, resulting in a scope of 23 β-amino-alcohol products. Kinetic competition studies elucidated that the cyclohexyl groups accelerate the enantiodetermining HAT step. Computational studies establish a network of hydrogen bonds, π-π stacking interactions, and London dispersion interactions as key noncovalent interactions that govern the high degrees of enantioinduction observed experimentally.

This work provides one of few examples of asymmetric HAT from a small-molecule catalyst. The mechanistic studies presented herein contribute to the growing body of literature on radical-based asymmetric catalysis, informing on how NCIs govern such enantioselectivity. Due to the highly modular nature of the peptide thiol catalysts disclosed herein and the ubiquity of HAT as an elementary step, we are optimistic that these catalysts may be further developed to effect asymmetric HAT with a structural diversity of prochiral radicals. Studies into other systems compatible with asymmetric HAT, as well as additional computational research into the conformational effects which dictate substrate-peptide interactions, are currently underway in our laboratories.

Supplementary Material

Refer to Web version on PubMed Central for supplementary material.

ACKNOWLEDGMENT

J.M.G. acknowledges Bristol Myers Squibb for a graduate fellowship. We thank Anthony Metrano and Nicholas Chiappini for helpful discussions. We thank Glenn Atkinson, the Princeton Physics Machine Shop, Brian Koronkiewicz, and Jackson Deobald for assistance with photoreactor design and construction. We also thank Ken Conover (PhotoNMR), István Pelczer (PhotoNMR), and Phil Jeffrey (X-ray Crystallography). DFT calculations were performed on the IDRE Hoffman2 cluster at the University of California, Los Angeles, and the Extreme Science and Engineering Discovery Environment (XSEDE), which is supported by the NSF (OCI1053575).

Funding Sources

Funding for this work was provided by the NIH (R35 GM134893 to R.R.K.) and (NIGMS R35 132092 to S.J.M), and the NSF (CHE-2153972 to K.N.H.).

REFERENCES

(1). (a)Tucker JW; Stephenson CRJ Shining Light on Photoredox Catalysis: Theory and Synthetic Applications. J. Org. Chem. 2012, 77 (4), 1617–1622. [PubMed: 22283525] (b)Shaw MH; Twilton J; MacMillan DWC Photoredox Catalysis in Organic Chemistry. J. Org. Chem. 2016, 81 (16), 6898–6926. [PubMed: 27477076] (c)Cahoon SB; Yoon TP Photochemistry and Radical Generation: Approaches in Mechanism Elucidation. In *Science of Synthesis*; Georg Thieme Verlag, 2020; 4, pp 159–205.

(2). (a)Nagib DA Asymmetric Catalysis in Radical Chemistry. Chem. Rev. 2022, 122 (21), 15989–15992. [PubMed: 36349458] (b)Mondal S; Dumur F; Gigmes D; Sibi MP; Bertrand MP; Nechab M Enantioselective Radical Reactions Using Chiral Catalysts. Chem. Rev. 2022, 122 (6), 5842–5976. [PubMed: 35073048] (c)Proctor RSJ; Colgan AC; Phipps RJ Exploiting Attractive Non-Covalent Interactions for the Enantioselective Catalysis of Reactions Involving Radical Intermediates. Nat. Chem. 2020, 12 (11), 990–1004. [PubMed: 33077927] (d)Silvi M; Melchiorre P Enhancing the Potential of Enantioselective Organocatalysis with Light. Nature 2018, 554 (7690), 41–49. [PubMed: 29388950]

Author Manuscript Author Manuscript Author Manuscript Author Manuscript

(3). (a)Dénès F; Pichowicz M; Povie G; Renaud P Thiyl Radicals in Organic Synthesis. Chem. Rev. 2014, 114 (5), 2587–2693. [PubMed: 24383397] (b)Sibi MP; Manyem S; Zimmerman J Enantioselective Radical Processes. Chem. Rev. 2003, 103 (8), 3263–3295. [PubMed: 12914498] (c)Studer A; Curran DP Catalysis of Radical Reactions: A Radical Chemistry Perspective. Angew. Chem. Int. Ed. 2016, 55 (1), 58–102.

(4). Zimmerman J; Sibi MP Enantioselective Radical Reactions. In Topics in Current Chemistry; Springer, 2006; 263, 107–162.

(5). For examples of asymmetric HAT mediated by a chiral Lewis acid or complexing agent, see: (a)Sibi MP; Patil K Enantioselective H-Atom Transfer Reaction: A Strategy to Synthesize Formaldehyde Aldol Products. Org. Lett. 2005, 7 (8), 1453–1456. [PubMed: 15816725] (b)Murakata M; Tsutsui H; Hoshino O Enantioselective Radical-Mediated Reduction of α-Iodolactone Using Tributyltin Hydride in the Presence of a Chiral Amine and a Lewis Acid. J. Chem. Soc. Chem. Commun. 1995, 48 (4), 481–482.(c)Sibi MP; Asano Y; Sausker JB Enantioselective Hydrogen Atom Transfer Reactions: Synthesis Of N-Acyl-α-Amino Acid Esters. Angew. Chemie Int. Ed. 2001, 40 (7), 1293–1296.(d)Sibi MP; Sausker JB The Role of the Achiral Template in Enantioselective Transformations. Radical Conjugate Additions to α-Methacrylates Followed by Hydrogen Atom Transfer. J. Am. Chem. Soc. 2002, 124 (6), 984–991. [PubMed: 11829606] (e)Murakata M; Tsutsui H; Takeuchi N; Hoshino O Enantioselective Radical-Mediated Reduction of α-Alkyl-α- Iododihydrocoumarins in the Presence of a Chiral Magnesium Iodide. Tetrahedron 1999, 55 (34), 10295–10304.(f)Urabe H; Yamashita K; Suzuki K; Kobayashi K; Sato F Lewis Acid-Enhanced Reactivity of α,β-Unsaturated Ester and Amide toward Radical Addition. J. Org. Chem. 1995, 60 (12), 3576–3577.(g)Sugimoto H; Nakamura S; Watanabe Y; Toru T Enantioselective Hydrogen Atom Transfer to α-Sulfonyl Radicals Controlled by Selective Coordination of a Chiral Lewis Acid to an Enantiotopic Sulfonyl Oxygen. Tetrahedron Asymmetry 2003, 14 (19), 3043–3055.(h)Sibi MP; Patil K Enantioselective H-Atom Transfer Reactions: A New Methodology for the Synthesis of β^2-Amino Acids. Angew. Chem. Int. Ed. 2004, 43 (10), 1235–1238.(i)Xu Z; Shen J; Li L; Chen W; Li S; Jiang J; Zhang YQ (Salen)Titanium-Catalyzed Asymmetric Hydrogen Atom Transfer for Epoxides Reduction. Angew. Chem. Int. Ed. 2022, 61 (50), e202214111.(j)Aechtner T; Dressel M; Bach T Hydrogen Bond Mediated Enantioselectivity of Radical Reactions. Angew. Chemie - Int. Ed. 2004, 43 (43), 5849–5851.(k)Großkopf J; Plaza M; Seitz A; Breitenlechner S; Storch G; Bach T Photochemical Deracemization at sp^3-Hybridized Carbon Centers via a Reversible Hydrogen Atom Transfer. J. Am. Chem. Soc. 2021, 143 (50), 21241–21245. [PubMed: 34902253]

(6). For examples of substrate-controlled stereoselective HAT from achiral H-atom donors, see: (a)Dang HS; Roberts BP Selective Radical-Chain Epimerisation at C-H Centres α to Oxygen under Conditions of Polarity-Reversal Catalysis. Tetrahedron Lett. 1999, 40 (22), 4271–4274. (b)Wang Y; Hu X; Morales-Rivera CA; Li GX; Huang X; He G; Liu P; Chen G Epimerization of Tertiary Carbon Centers via Reversible Radical Cleavage of Unactivated C(sp3)-H Bonds. J. Am. Chem. Soc. 2018, 140 (30), 9678–9684. [PubMed: 29983059] (c)Wang Y; Carder HM; Wendlandt AE Synthesis of Rare Sugar Isomers through Site-Selective Epimerization. Nature 2020, 578 (7795), 403–408. [PubMed: 31940659] (d)Zhang YA; Gu X; Wendlandt AE A Change from Kinetic to Thermodynamic Control Enables Trans-Selective Stereochemical Editing of Vicinal Diols. J. Am. Chem. Soc. 2022, 144 (1), 599–605. [PubMed: 34928134] (e)Zhang YA; Palani V; Seim AE; Wang Y; Wang KJ; Wendlandt AE Stereochemical Editing Logic Powered by the Epimerization of Unactivated Tertiary Stereocenters. Science, 2022, 378 (6618), 383–390. [PubMed: 36302032] (f)Oswood CJ; MacMillan DWC Selective Isomerization via Transient Thermodynamic Control: Dynamic Epimerization of Trans to Cis Diols. J. Am. Chem. Soc. 2022, 144 (1), 93–98. [PubMed: 34933555] (g)Kazerouni AM; Brandes DS; Davies CC; Cotter LF; Mayer JM; Chen S; Ellman JA Visible Light-Mediated, Highly Diastereoselective Epimerization of Lactams from the Most Accessible to the More Stable Stereoisomer. ACS Catal. 2022, 12 (13), 7798–7803. [PubMed: 35832573]

(7). For an example of diastereoselective HAT from a chiral thiol catalyst, see:Brill ZG; Grover HK; Maimone TJ. Enantioselective Synthesis of an Ophiobolin Sesterterpene via a Programmed Radical Cascade. Science 2016, 352 (6289), 1078–1082. [PubMed: 27230373]

(8). (a)Schumann H; Pachaly B; Schütze BC Asymmetrische Diorganoalkoxyzinnhydride Und Ihre Anwendung Als Stereoselektive Reduktionsmittel. J. Organomet. Chem. 1984, 265 (2), 146–

Author Manuscript Author Manuscript Author Manuscript Author Manuscript

152.(b)Nanni D; Curran DP Synthesis and Some Reactions of the First Chiral Tin Hydride Containing a C_2-Symmetric Binaphthyl Substituent. Tetrahedron Asymmetry 1996, 7 (8), 2417–2422.(c)Blumenstein M; Schwarzkopf K; Metzger JO Enantioselective Hydrogen Transfer from a Chiral Tin Hydride to a Prochiral Carbon-Centered Radical. Angew. Chem. Int. Ed. 1997, 36 (3), 235–236.(d)Dakternieks D; Dunn K; Perchyonok VT; Schiesser CH Remarkable Lewis Acid Mediated Enhancement of Enantioselectivity during Free-Radical Reductions by Simple Chiral Non-Racemic Stannanes. Chem. Commun. 1999, 17, 1665–1666.(e)Kang J; Kim TH Asymmetric Radical Reduction with Planar Chiral Organotin Hydrides. Bull. Korean Chem. Soc. 2003, 24 (8), 1055–1056.(f)Schiesser CH; Skidmore MA; White JM Stannanes from Cholic Acid as Enantioselective Free-Radical Reducing Agents. Aust. J. Chem. 2001, 54 (3), 199–204.(g)Dakternieks D; Schiesser CH The Quest for Single-Enantiomer Outcomes in Free-Radical Chemistry. Aust. J. Chem. 2001, 54 (2), 89–91.For an example of the same reactivity with chiral germanes, see:(h)Zeng L; Dakternieks D; Duthie A; Perchyonok T; Schiesser C Synthesis, Characterization and Enantioselective Free Radical Reductions of (1R,2S,5R)-Menthyldiphenylgermane and Its Enantiomer. Tetrahedron Asymmetry 2004, 15 (16), 2547–2554.

(9). (a)Haque MB; Roberts BP Enantioselective Radical-Chain Hydrosilylation of Prochiral Alkenes Using Optically Active Thiol Catalysts. Tetrahedron Lett. 1996, 37 (50), 9123–9126.(b)Haque MB; Roberts BP; Tocher DA Enantioselective Radical-Chain Hydrosilylation of Alkenes Using Homochiral Thiols as Polarity-Reversal Catalysts. J. Chem. Soc. - Perkin Trans. 1 1998, 10 (17), 2881–2889.

(10). Ramanathan D; Shi Q; Xu M; Chang R; Peñín B; Funes-Ardoiz I; Ye J Catalytic Asymmetric Deuterosilylation of Exocyclic Olefins with Mannose-Derived Thiols and Deuterium Oxide. Org. Chem. Front. 2023, 10 (5), 1182–1190.

(11). (a)Cotruvo JA; Stubbe J Class I Ribonucleotide Reductases: Metallocofactor Assembly and Repair in Vitro and in Vivo. Annu. Rev. Biochem. 2011, 80, 733–767. [PubMed: 21456967] (b)Broderick JB; Duffus BR; Duschene KS; Shepard EM Radical S-Adenosylmethionine Enzymes. Chem. Rev. 2014, 114 (8), 4229–4317. [PubMed: 24476342] (c)Kudo F; Hoshi S; Kawashima T; Kamachi T; Eguchi T Characterization of a Radical S-Adenosyl-L-Methionine Epimerase, NeoN, in the Last Step of Neomycin B Biosynthesis. J. Am. Chem. Soc. 2014, 136 (39), 13909–13915. [PubMed: 25230155]

(12). McLean JT; Benny A; Nolan MD; Swinand G; Scanlan EM Cysteinyl Radicals in Chemical Synthesis and in Nature. Chem. Soc. Rev. 2021, 50 (19), 10857–10894. [PubMed: 34397045]

(13). (a)Nakano Y; Biegasiewicz KF; Hyster TK Biocatalytic Hydrogen Atom Transfer: An Invigorating Approach to Free-Radical Reactions. Curr. Opin. Chem. Biol. 2019, 49, 16–24. [PubMed: 30269010] (b)Emmanuel MA; Greenberg NR; Oblinsky DG; Hyster TK Accessing Non-Natural Reactivity by Irradiating Nicotinamide-Dependent Enzymes with Light. Nature 2016, 540 (7633), 414–417. [PubMed: 27974767] (c)Sandoval BA; Meichan AJ; Hyster TK Enantioselective Hydrogen Atom Transfer: Discovery of Catalytic Promiscuity in Flavin-Dependent 'Ene'-Reductases. J. Am. Chem. Soc. 2017, 139 (33), 11313–11316. [PubMed: 28780870] (d)Nakano Y; Black MJ; Meichan AJ; Sandoval BA; Chung MM; Biegasiewicz KF; Zhu T; Hyster TK Photoenzymatic Hydrogenation of Heteroaromatic Olefins Using 'Ene'-Reductases with Photoredox Catalysts. Angew. Chem. Int. Ed. 2020, 59 (26), 10484–10488.(e)Clayman PD; Hyster TK Photoenzymatic Generation of Unstabilized Alkyl Radicals: An Asymmetric Reductive Cyclization. J. Am. Chem. Soc. 2020, 142 (37), 15673–15677. [PubMed: 32857506] (f)Huang X; Wang B; Wang Y; Jiang G; Feng J; Zhao H Photoenzymatic Enantioselective Intermolecular Radical Hydroalkylation. Nature 2020, 584 (7819), 69–74. [PubMed: 32512577] (g)Fu H; Lam H; Emmanuel MA; Kim JH; Sandoval BA; Hyster TK Ground-State Electron Transfer as an Initiation Mechanism for Biocatalytic C-C Bond Forming Reactions. J. Am. Chem. Soc. 2021, 143 (25), 9622–9629. [PubMed: 34114803] (h)Page CG; Cooper SJ; Dehovitz JS; Oblinsky DG; Biegasiewicz KF; Antropow AH; Armbrust KW; Ellis JM; Hamann LG; Horn EJ; Oberg KM; Scholes GD; Hyster TK Quaternary Charge-Transfer Complex Enables Photoenzymatic Intermolecular Hydroalkylation of Olefins. J. Am. Chem. Soc. 2021, 143 (1), 97–102. [PubMed: 33369395] (i)Huang X; Feng J; Cui J; Jiang G; Harrison W; Zang X; Zhou J; Wang B; Zhao H Photoinduced Chemomimetic Biocatalysis for Enantioselective Intermolecular Radical Conjugate Addition. Nat. Catal. 2022, 5 (7), 586–

Author Manuscript Author Manuscript Author Manuscript Author Manuscript

593.(j)Fu H; Cao J; Qiao T; Qi Y; Charnock SJ; Garfinkle S; Hyster TK An Asymmetric sp3–sp3 Cross-Electrophile Coupling Using 'Ene'-Reductases. Nature 2022, 610 (7931), 302–307. [PubMed: 35952713] (k)Ye Y; Cao J; Oblinsky DG; Verma D; Prier CK; Scholes GD; Hyster TK Using Enzymes to Tame Nitrogen-Centred Radicals for Enantioselective Hydroamination. Nat. Chem. 2022, 15 (2), 206–212. [PubMed: 36376390]

(14). (a)Davie EAC; Mennen SM; Xu Y; Miller SJ Asymmetric Catalysis Mediated by Synthetic Peptides. Chem. Rev. 2007, 107 (12), 5759–5812. [PubMed: 18072809] (b)Metrano AJ; Chinn AJ; Shugrue CR; Stone EA; Kim B; Miller SJ Asymmetric Catalysis Mediated by Synthetic Peptides, Version 2.0: Expansion of Scope and Mechanisms. Chem. Rev. 2020, 120 (20), 11479–11615. [PubMed: 32969640] (c)Lewandowski B; Wennemers H Asymmetric Catalysis with Short-Chain Peptides. Curr. Opin. Chem. Biol. 2014, 22, 40–46. [PubMed: 25277500] (d)Wennemers H Peptides – Molecular Allrounders. Chimia 2021, 75 (6), 525–529. [PubMed: 34233818] (e)Wennemers H Asymmetric Catalysis with Peptides. Chem. Commun. 2011, 47 (44), 12036–12041.

(15). Shin NY; Ryss JM; Zhang X; Miller SJ; Knowles RR Light-Driven Deracemization Enabled by Excited-State Electron Transfer. Science 2019, 366 (6463), 364–369. [PubMed: 31624212]

(16). Shi Q; Xu M; Chang R; Ramanathan D; Peñin B; Funes-Ardoiz I; Ye J Visible-Light Mediated Catalytic Asymmetric Radical Deuteration at Non-Benzylic Positions. Nat. Commun. 2022, 13 (1), 1–9. [PubMed: 34983933]

(17). Zhu Q; Graff DE; Knowles RR Intermolecular Anti-Markovnikov Hydroamination of Unactivated Alkenes with Sulfonamides Enabled by Proton-Coupled Electron Transfer. J. Am. Chem. Soc. 2018, 140 (2), 741–747. [PubMed: 29268020]

(18). CYLview20; Legault CY, Université de Sherbrooke, 2020 (http://cylview.org)

(19). (a)Knowles RR; Jacobsen EN Attractive Noncovalent Interactions in Asymmetric Catalysis: Links between Enzymes and Small Molecule Catalysts. Proc. Natl. Acad. Sci. U. S. A. 2010, 107 (48), 20678–20685. [PubMed: 20956302] (b)Raghothama SR; Awasthi SK; Balaram P β-Hairpin Nucleation by Pro-Gly β-Turns. Comparison of D-Pro-Gly and L-Pro-Gly Sequences in an Apolar Octapeptide. J. Chem. Soc. Perkin Trans. 2 1998, 2 (1), 137–143.

(20). For selected examples of asymmetric radical functionalization guided by hydrogen bonding and other NCIs, see:(a)Uraguchi D; Kinoshita N; Kizu T; Ooi T Synergistic Catalysis of Ionic Brønsted Acid and Photosensitizer for a Redox Neutral Asymmetric α-Coupling of *N*-Arylaminomethanes with Aldimines. J. Am. Chem. Soc. 2015, 137 (43), 13768–13771. [PubMed: 26456298] (b)Lin L; Bai X; Ye X; Zhao X; Tan CH; Jiang Z Organocatalytic Enantioselective Protonation for Photoreduction of Activated Ketones and Ketimines Induced by Visible Light. Angew. Chem. Int. Ed. 2017, 56 (44), 13842–13846.(c)Wang Y; Wen X; Cui X; Wojtas L; Zhang XP Asymmetric Radical Cyclopropanation of Alkenes with in Situ-Generated Donor-Substituted Diazo Reagents via Co(II)-Based Metalloradical Catalysis. J. Am. Chem. Soc. 2017, 139 (3), 1049–1052. [PubMed: 28051870] (d)Proctor RSJ; Davis HJ; Phipps RJ Catalytic Enantioselective Minisci-Type Addition to Heteroarenes. Science 2018, 360 (6387), 419–422. [PubMed: 29622723] (e)Cao K; Tan SM; Lee R; Yang S; Jia H; Zhao X; Qiao B; Jiang Z Catalytic Enantioselective Addition of Prochiral Radicals to Vinylpyridines. J. Am. Chem. Soc. 2019, 141 (13), 5437–5443. [PubMed: 30866625] (f)Roos CB; Demaerel J; Graff DE; Knowles RR Enantioselective Hydroamination of Alkenes with Sulfonamides Enabled by Proton-Coupled Electron Transfer. J. Am. Chem. Soc. 2020, 142 (13), 5974–5979. [PubMed: 32182054] (g)Gu QS; Li ZL; Liu XY Copper(I)-Catalyzed Asymmetric Reactions Involving Radicals. Acc. Chem. Res. 2020, 53 (1), 170–181. [PubMed: 31657546] (h)Turek AK; Sak MH; Miller SJ Kinetic Analysis of a Cysteine-Derived Thiyl-Catalyzed Asymmetric Vinylcyclopropane Cycloaddition Reflects Numerous Attractive Noncovalent Interactions. J. Am. Chem. Soc. 2021, 143 (39), 16173–16183. [PubMed: 34553915] (i)Chapman SJ; Swords WB; Le CM; Guzei IA; Toste FD; Yoon TP Cooperative Stereoinduction in Asymmetric Photocatalysis. J. Am. Chem. Soc. 2022, 144 (9), 4206–4213. [PubMed: 35192768]

(21). (a)Wilmot CM; Thornton JM Analysis and Prediction of the Different Types of β-Turn in Proteins. J. Mol. Biol. 1988, 203 (1), 221–232. [PubMed: 3184187] (b)Hutchinson EG; Thornton JM A Revised Set of Potentials for β-Turn Formation in Proteins. Protein Sci. 1994, 3 (12), 2207–2216. [PubMed: 7756980] (c)Metrano AJ; Abascal NC; Mercado BQ; Paulson EK; Hurtley AE; Miller SJ Diversity of Secondary Structure in Catalytic Peptides with β-Turn-Biased

Author Manuscript Author Manuscript Author Manuscript Author Manuscript

Sequences. J. Am. Chem. Soc. 2017, 139 (1), 492–516. [PubMed: 28029251] (d)Copeland GT; Jarvo ER; Miller SJ Minimal Acylase-like Peptides. Conformational Control of Absolute Stereospecificity. J. Org. Chem. 1998, 63 (20), 6784–6785. [PubMed: 11672295]

(22). (a)Gallo EA; Gellman SH Hydrogen-Bond-Mediated Folding in Depsipeptide Models of β-Turns and α-Helical Turns. J. Am. Chem. Soc. 1993, 115 (21), 9774–9788.(b)Haque TS; Little JC; Gellman SH "Mirror Image" Reverse Turns Promote β-Hairpin Formation. J. Am. Chem. Soc. 1994, 116 (9), 4105–4106.(c)Haque TS; Little JC; Gellman SH Stereochemical Requirements for β-Hairpin Formation: Model Studies with Four-Residue Peptides and Depsipeptides. J. Am. Chem. Soc. 1996, 118 (29), 6975–6985.(d)Hurtley AE; Stone EA; Metrano AJ; Miller SJ Desymmetrization of Diarylmethylamido Bis(Phenols) through Peptide-Catalyzed Bromination: Enantiodivergence as a Consequence of a 2 amu Alteration at an Achiral Residue within the Catalyst. J. Org. Chem. 2017, 82 (21), 11326–11336. [PubMed: 29020446]

(23). Joaquin D; Lee MA; Kastner DW; Singh J; Morrill ST; Damstedt G; Castle SL Impact of Dehydroamino Acids on the Structure and Stability of Incipient 310-Helical Peptides. J. Org. Chem. 2020, 85 (3), 1601–1613. [PubMed: 31730750]

(24). (a)Stone EA; Hosseinzadeh P; Craven TW; Robertson MJ; Han Y; Hsieh SY; Metrano AJ; Baker D; Miller SJ Isolating Conformers to Assess Dynamics of Peptidic Catalysts Using Computationally Designed Macrocyclic Peptides. ACS Catal. 2021, 11 (8), 4395–4400. [PubMed: 34659874] (b)Crawford JM; Sigman MS Conformational Dynamics in Asymmetric Catalysis: Is Catalyst Flexibility a Design Element? Synthesis 2019, 51 (5), 1021–1036. [PubMed: 31235980]

(25). Kwon Y; Li J; Reid JP; Crawford JM; Jacob R; Sigman MS; Toste FD; Miller SJ Disparate Catalytic Scaffolds for Atroposelective Cyclodehydration. J. Am. Chem. Soc. 2019, 141 (16), 6698–6705. [PubMed: 30920223]

(26). (a)Wheeler SE; Houk KN Substituent Effects in the Benzene Dimer Are Due to Direct Interactions of the Substituents with the Unsubstituted Benzene. J. Am. Chem. Soc. 2008, 130 (33), 10854–10855. [PubMed: 18652453] (b)Wheeler SE; Houk KN Through-Space Effects of Substituents Dominate Molecular Electrostatic Potentials of Substituted Arenes. J. Chem. Theory Comput. 2009, 5 (9), 2301–2312. [PubMed: 20161573]

(27). These two mechanistic scenarios are not mutually exclusive; the more selective catalyst could both increase the barrier to the minor enantiomer and decrease the barrier to the major enantiomer. Similarly, the catalyst could lower or raise both barriers, though by a greater degree for one enantiomer versus the other. Nonetheless, in any of these mechanistic scenarios, a nonstatistical selectivity biased towards that of the more selective catalyst can only be achieved in a scenario in which the barrier to the major enantiomer is lowered relative to that of the less selective catalyst.

(28). For an example of such an experiment, see:Eschmann C; Song L; Schreiner PR. London Dispersion Interactions Rather than Steric Hindrance Determine the Enantioselectivity of the Corey–Bakshi–Shibata Reduction. Angew. Chem. Int. Ed. 2021, 60 (9), 4823–4832.

(29). (a)Xu EY; Werth J; Roos CB; Bendelsmith AJ; Sigman MS; Knowles RR Noncovalent Stabilization of Radical Intermediates in the Enantioselective Hydroamination of Alkenes with Sulfonamides. J. Am. Chem. Soc. 2022, 144 (41), 18948–18958. [PubMed: 36197450] (b)Qin Y; Zhu Q; Sun R; Ganley JM; Knowles RR; Nocera DG Mechanistic Investigation and Optimization of Photoredox Anti-Markovnikov Hydroamination. J. Am. Chem. Soc. 2021, 143 (27), 10232–10242. [PubMed: 34191486]

(30). Frisch MJ; Trucks GW; Schlegel HB; Scuseria GE; Robb MA; Cheeseman JR; Scalmani G; Barone V; Petersson GA; Nakatsuji H; Li X; Caricato M; Marenich AV; Bloino J; Janesko BG; Gomperts R; Mennucci B; Hratchian HP; Ortiz JV; Izmaylov AF; Sonnenberg JL; Williams-Young D, Ding F; Lipparini F; Egidi F; Goings J; Peng B; Petrone A; Henderson T; Ranasinghe D; Zakrzewski VG; Gao J; Rega N; Zheng G; Liang W; Hada M; Ehara M; Toyota K; Fukuda R; Hasegawa J; Ishida M; Nakajima T; Honda Y; Kitao O; Nakai H; Vreven T; Throssell K; Montgomery JA Jr., Peralta JE; Ogliaro F; Bearpark MJ; Heyd JJ; Brothers EN; Kudin KN; Staroverov VN; Keith TA; Kobayashi R; Normand J; Raghavachari K; Rendell AP; Burant JC; Iyengar SS; Tomasi J; Cossi M; Millam JM; Klene M; Adamo C; Cammi R; Ochterski JW; Martin RL; Morokuma K; Farkas O; Foresman JB; Fox DJ Gaussian 16, Revision A.03; Gaussian, Inc.: Wallingford, CT, 2016.

Author Manuscript Author Manuscript Author Manuscript Author Manuscript

(31). Chai J. Da; Head-Gordon M. Long-Range Corrected Hybrid Density Functionals with Damped Atom-Atom Dispersion Corrections. Phys. Chem. Chem. Phys. 2008, 10 (44), 6615–6620. [PubMed: 18989472]

(32). Weigend F; Ahlrichs R Balanced Basis Sets of Split Valence, Triple Zeta Valence and Quadruple Zeta Valence Quality for H to Rn: Design and Assessment of Accuracy. Phys. Chem. Chem. Phys. 2005, 7 (18), 3297–3305. [PubMed: 16240044]

(33). (a)Barone V; Cossi M Quantum Calculation of Molecular Energies and Energy Gradients in Solution by a Conductor Solvent Model. J. Phys. Chem. A 1998, 102 (11), 1995–2001.(b)Cossi M; Rega N; Scalmani G; Barone V Energies, Structures, and Electronic Properties of Molecules in Solution with the C-PCM Solvation Model. J. Comput. Chem. 2003, 24 (6), 669–681. [PubMed: 12666158]

(34). Wohlfarth C Permittivity (Dielectric Constant) of Liquids. In CRC Handbook of Chemistry and Physics, 97th ed.; Haynes WM, Lide DR, Bruno TJ, Eds.; CRC, Press: Boca Raton, FL, 2016; pp 6–199.

(35). Pracht P; Bohle F; Grimme S Automated Exploration of the Low-Energy Chemical Space with Fast Quantum Chemical Methods. Phys. Chem. Chem. Phys. 2020, 22 (14), 7169–7192. [PubMed: 32073075]

(36). Grimme S Supramolecular Binding Thermodynamics by Dispersion-Corrected Density Functional Theory. Chem. Eur. J. 2012, 18 (32), 9955–9964. [PubMed: 22782805]

(37). Luchini G; Alegre-Requena JV; Funes-Ardoiz I; Paton RS. GoodVibes: Automated Thermochemistry for Heterogeneous Computational Chemistry Data. F1000Research 2020, 9, 291.

(38). We note that conducting the hydroamination reaction at high dilution generally resulted in higher degrees of enantioselectivity (see SI Tables S9 and S11). Therefore, it is likely that some of this overestimation is due to effects of other reaction components which may be involved in the transition state, but were not incorporated in computational models.

(39). A similar interaction has been proposed in the following reference, demonstrating H–H distances of ~2.5 Å: Müller CE; Zell D; Hrdina R; Wende RC; Wanka L, Schuler SMM; Schreiner PR Lipohiplic Oligopeptides for Chemo- and Enantioselective Acyl Transfer Reactions onto Alcohols. J. Org. Chem. 2013, 78 (17), 8465–8484. [PubMed: 23875609]

(40). (a)Wagner JP; Schreiner PR London Dispersion in Molecular Chemistry - Reconsidering Steric Effects. Angew. Chem. Int. Ed. 2015, 54 (42), 12274–12296.(b)Wende RC; Seitz A; Niedek D; Schuler SMM; Hofmann C; Becker J; Schreiner PR The Enantioselective Dakin-West Reaction. Angew. Chem. Int. Ed. 2016, 55 (8), 2719–2723.

(41). Solel E; Ruth M; Schreiner PR London Dispersion Helps Refine Steric A-Values: Dispersion Energy Donor Scales. J. Am. Chem. Soc. 2021, 143 (49), 20837–20848. [PubMed: 34846890]

(42). Contreras-Garcia J; Johnson R,E; Keinan S; Chaudret R; Piquemal J-P; Beratan D,N; Yang W. NCIPLOT: A Program for Plotting Noncovalent Interaction Regions. J. Chem. Theory. Comput. 2011, 7 (3), 625−632. [PubMed: 21516178]

(43). We note that while dispersion is reasonably a contributing factor to the improved enantioselectivity observed with P14, the dicyclohexylmethyl ether may also improve enantioselectivity through other means, such as stabilizing other NCIs (e.g. hydrogen-bonding) within the transition state or influencing the population of higher energy transition states.

Author Manuscript Author Manuscript Author Manuscript Author Manuscript

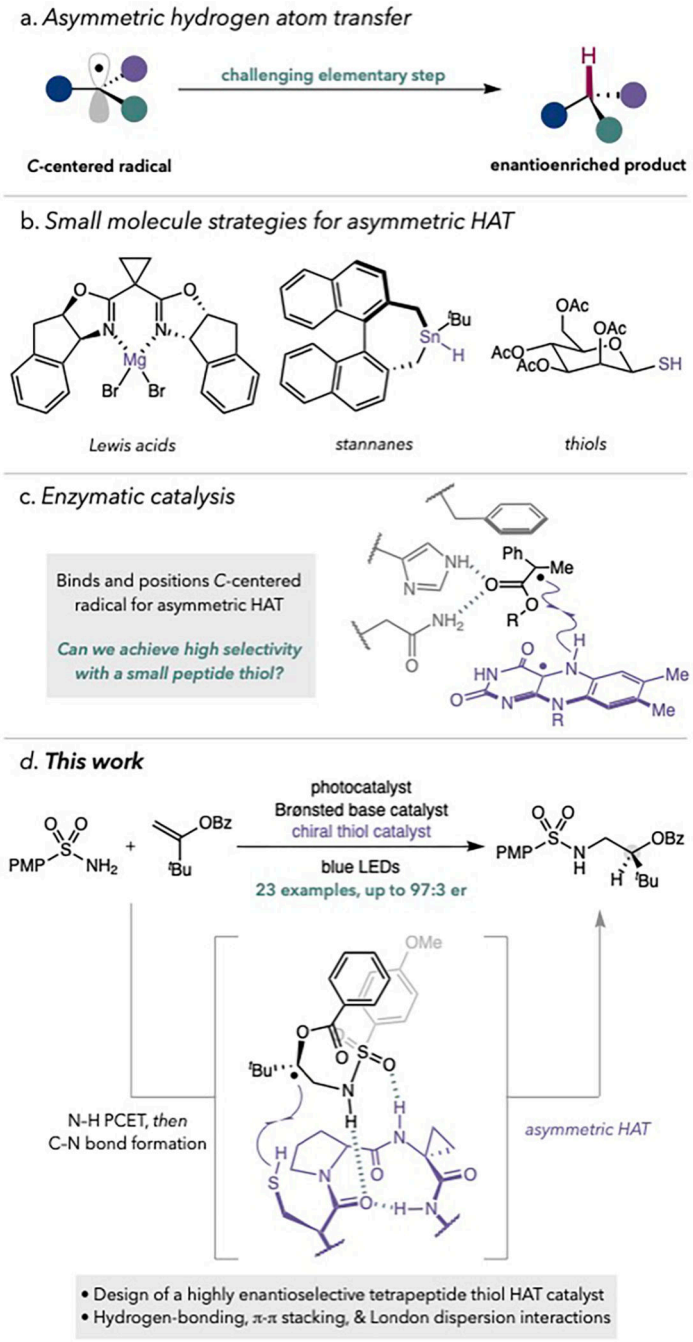

Figure 1.

a. Asymmetric HAT is an enabling, yet challenging elementary step. b. Small molecule approaches to achieve asymmetric HAT have employed chiral species such as Lewis acids, stannanes, and thiols. c. Enzymes bind and properly orient the prochiral radical intermediate for asymmetric HAT. d. *This work*: Enantioselective olefin hydroamination *via* asymmetric HAT from a peptide thiol catalyst.

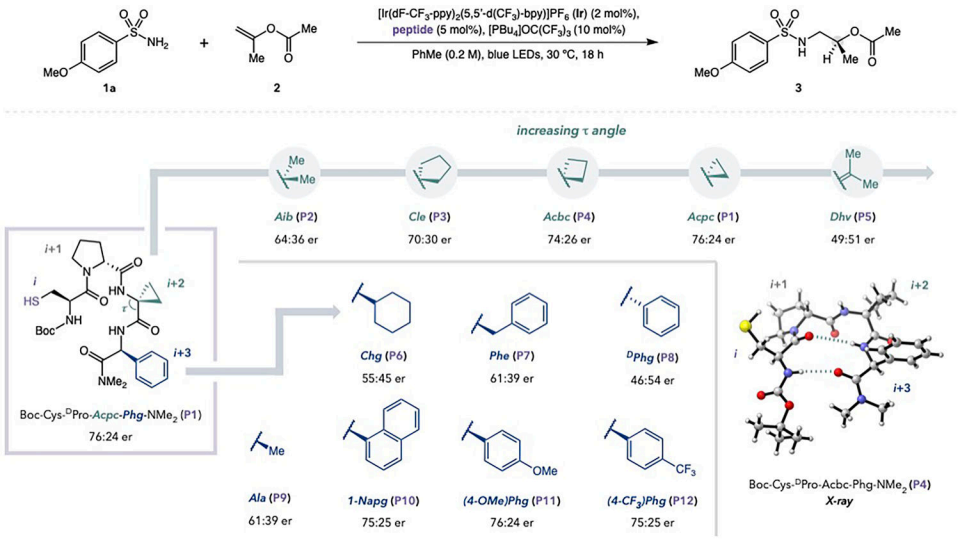

Figure 2.

Structure-selectivity relationships of peptide *i*+2 and *i*+3 residue variations. Reactions were conducted with 0.05 mmol **1a** and 3 equiv. **2**. The X-ray crystal structure of **P4** was rendered using CYLview.[18]

Author Manuscript Author Manuscript Author Manuscript Author Manuscript

Author Manuscript Author Manuscript Author Manuscript Author Manuscript

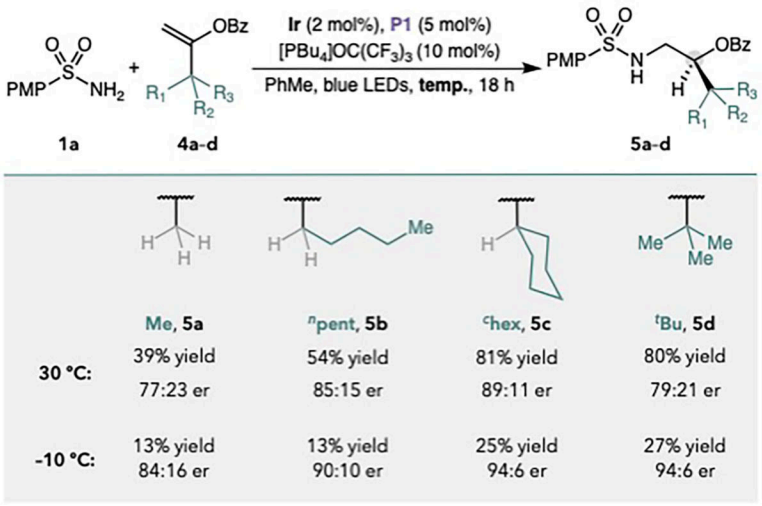

Figure 3.

Effect of alkyl group substitution and temperature on hydroamination yield and enantioselectivity.

Author Manuscript Author Manuscript Author Manuscript Author Manuscript

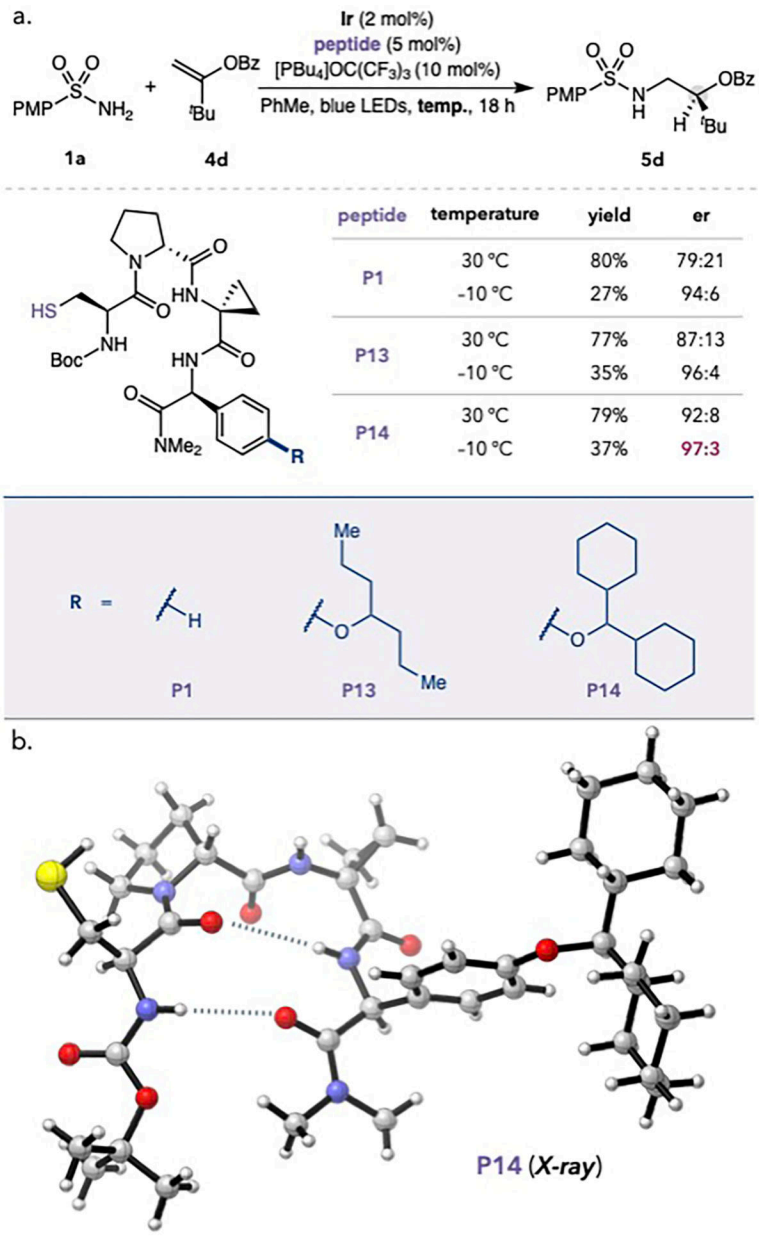

Figure 4.

a. Effects of temperature and peptide alkylation on hydroamination yield and enantioselectivity. b. X-ray crystal structure of **P14**, rendered using CYLview.[18]

Author Manuscript Author Manuscript Author Manuscript Author Manuscript

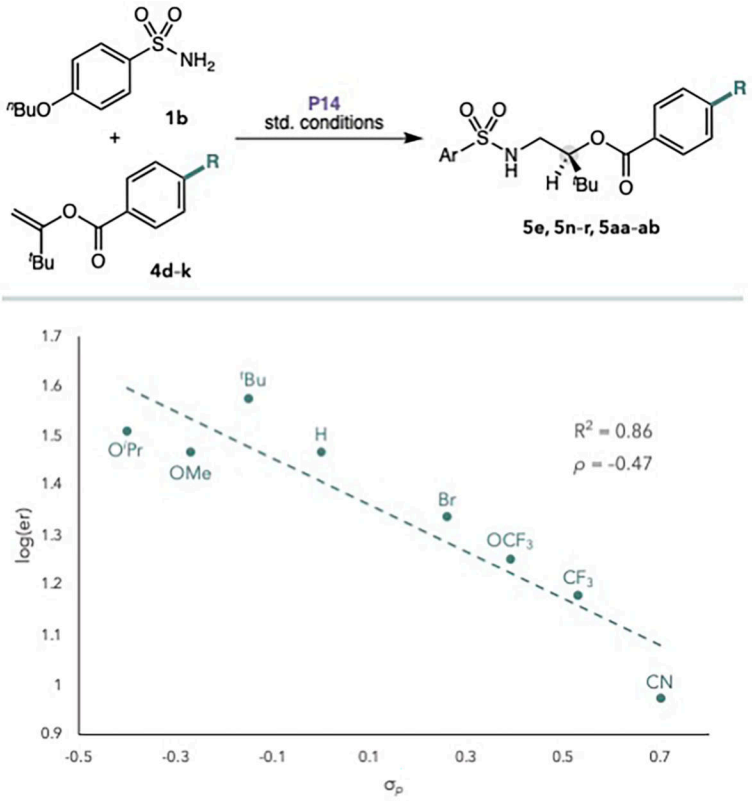

Figure 5.
Hammett study of *para*-substituted enol benzoates. See SI Table S5 for further details.

Author Manuscript Author Manuscript Author Manuscript Author Manuscript

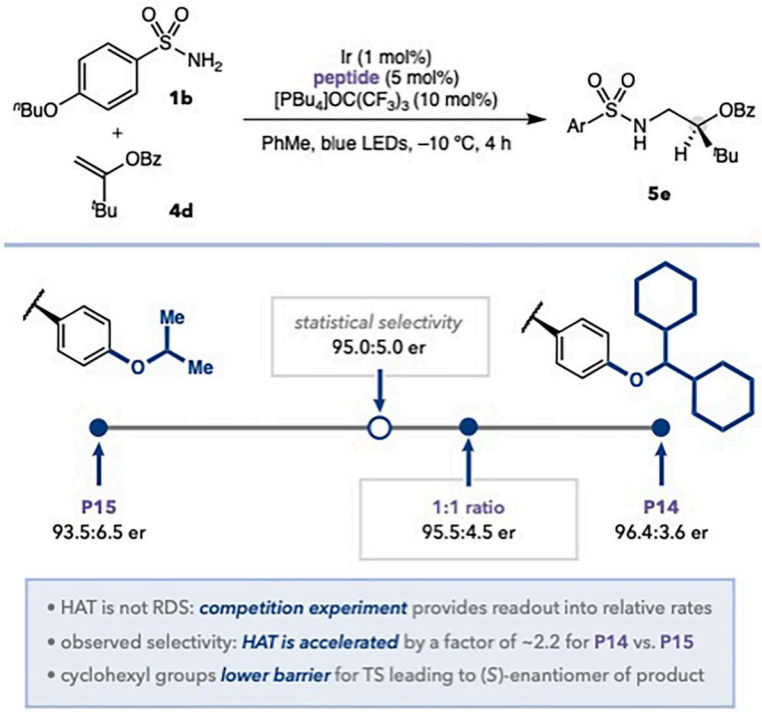

Figure 6.

Kinetic competition study between differentially substituted *i*↛3 residues to examine the rate effects of the Phg arene substituents on HAT. These results demonstrate a ~2.2-fold rate enhancement for peptide thiol catalyst **P14** vs. **P15**.

Author Manuscript Author Manuscript Author Manuscript Author Manuscript

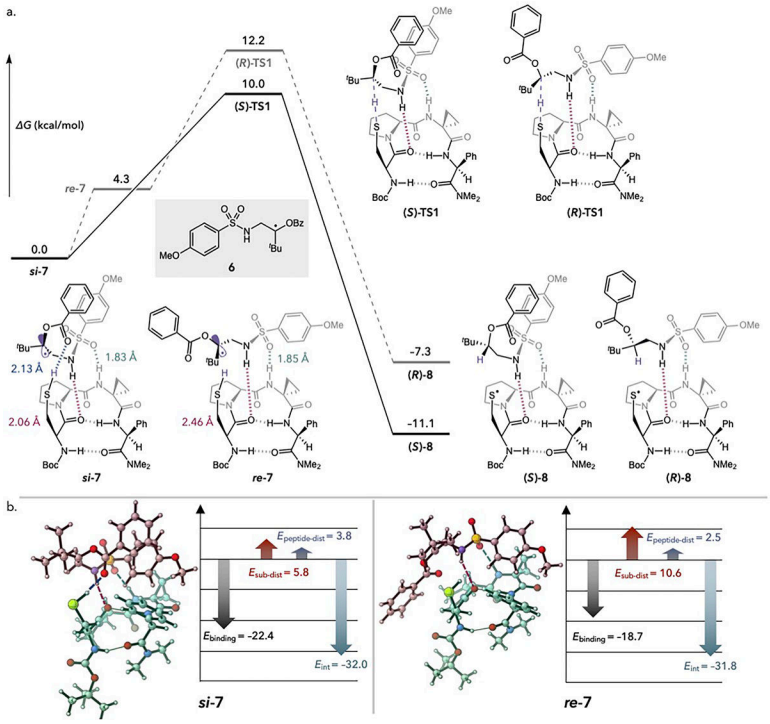

Figure 7.

a. Computed reaction coordinate profile of the hydrogen atom transfer step; b. Optimized geometries and distortion-interaction analysis of peptide-bound prochiral intermediates.

Author Manuscript Author Manuscript Author Manuscript Author Manuscript

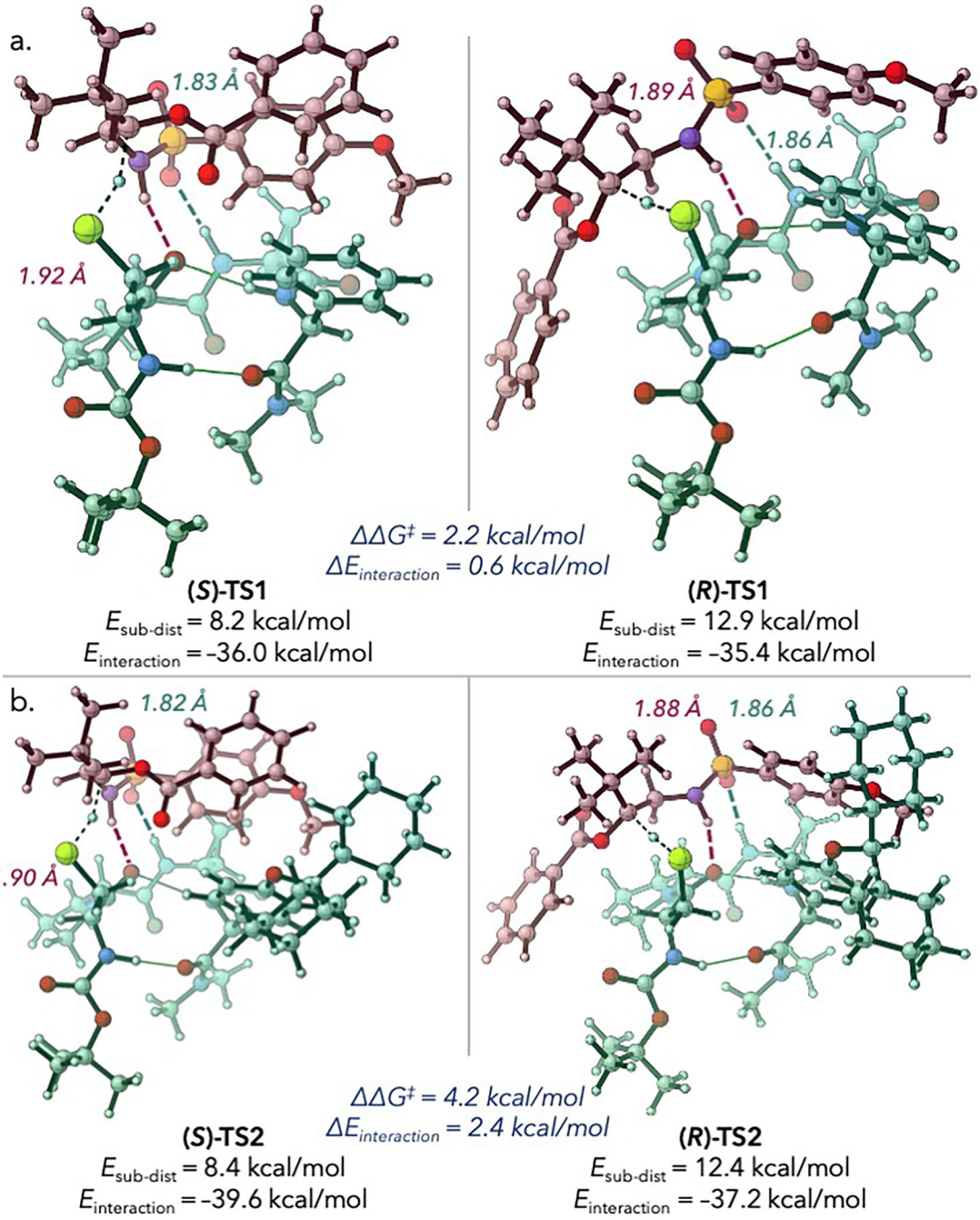

Figure 8.
Computed selectivity-determining transition state structures with peptide a. **P1**; and b. **P14**.

Author Manuscript Author Manuscript Author Manuscript Author Manuscript

J Am Chem Soc. Author manuscript; available in PMC 2024 July 26.

Table 1.

Substrate scope of asymmetric hydroamination

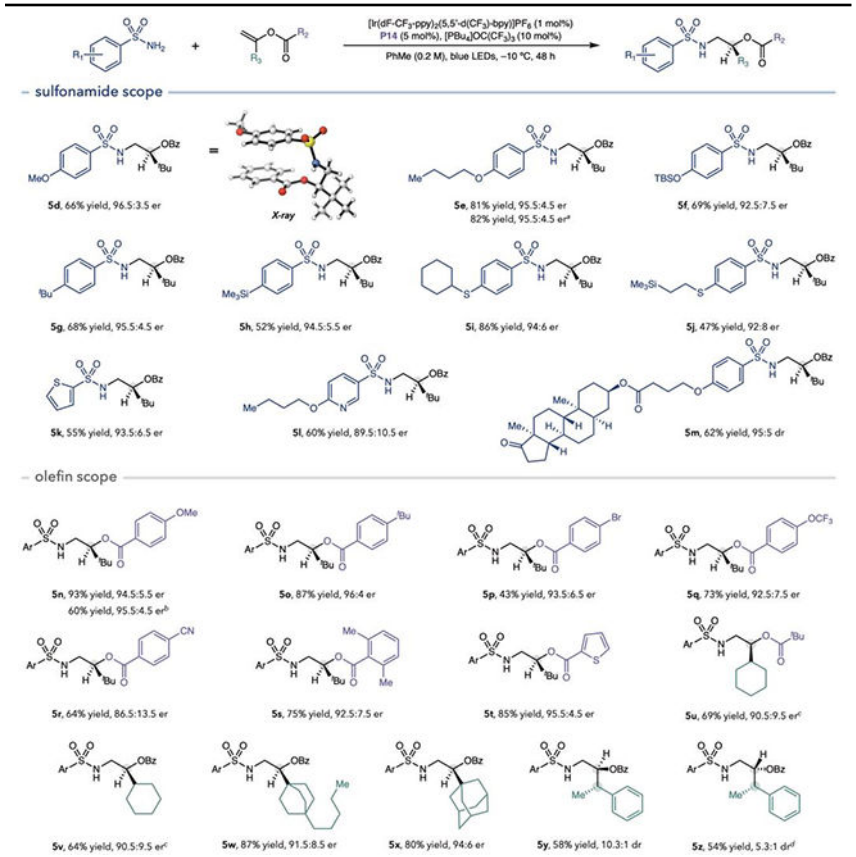

Yields and enantioselectivities are for isolated material and are the average of two experiments. Reactions were conducted on 0.3 mmol scale using 5 equiv. olefin. Ar = 4-(^{n}BuO)Ph. The X-ray crystal structure of **5d** was rendered using CYLview.[18]

[a] using 2 mol% **P14**

[b] using 2 equiv. olefin

[c] using 5 mol% **P13**

$d_{\text{using } \textbf{\textit{ent}}\text{-P14}}$

Author Manuscript Author Manuscript Author Manuscript Author Manuscript